PROCEEDINGS OF SPIE

SPIEDigitalLibrary.org/conference-proceedings-of-spie

Estimates for the background of the ATHENA X-IFU instrument: the cosmic rays contribution

Simone Lotti, Claudio Macculi, Matteo D'Andrea, Valentina Fioretti, Paolo Dondero, et al.

Simone Lotti, Claudio Macculi, Matteo D'Andrea, Valentina Fioretti, Paolo Dondero, Alfonso Mantero, Gabriele Minervini, Andrea Argan, Luigi Piro, "Estimates for the background of the ATHENA X-IFU instrument: the cosmic rays contribution," Proc. SPIE 10699, Space Telescopes and Instrumentation 2018: Ultraviolet to Gamma Ray, 106991Q (6 July 2018); doi: 10.1117/12.2313236

SPIE.

Event: SPIE Astronomical Telescopes + Instrumentation, 2018, Austin, Texas, United States

Estimates for the background of the ATHENA X-IFU instrument: the Cosmic Rays contribution

Simone Lotti[a], Claudio Macculi[a], Matteo D'Andrea[a], Valentina Fioretti[b], Paolo Dondero[c], Alfonso Mantero[c], Gabriele Minervini[a], Andrea Argan[a], and Luigi Piro[a]

[a]Istituto di Astrofisica e Planetologia Spaziali, Via fosso del cavaliere 100, Roma, Italia
[b]IASF Bologna, Via Piero Gobetti 101, Bologna, Italia
[c]SWHARD srl, Via Greto di Cornigliano 6r - box 39, 16152 Genova, Italia

ABSTRACT

The background of the ATHENA X-IFU instrument is evaluated by Geant4 simulations. A new, highly detailed, mass model of the X-IFU and of its cryostat has been produced, a new model for the Galactic Cosmic Ray protons in L2 has been developed from satellite data, and a set of physics models tuned to ATHENA needs has been refined through extensive validations against experimental results. We are going to report the latest results in the estimate of the background of the X-IFU instrument, obtained after the update of all the elements of the Geant4 simulations and of the post processing software.

Keywords: ATHENA, X-IFU, X-ray detectors, background, Geant4

1. INTRODUCTION

ATHENA is a large-class ESA X-ray mission with a launch foreseen in 2030 towards the L2 orbit. The mission addresses the science theme The Hot and Energetic Universe, by coupling a high-performance X-ray Telescope with two complementary focal-plane instruments. One of these, the X-ray Integral Field Unit (X-IFU) is a TES based kilo-pixel array, providing spatially resolved high-resolution spectroscopy (2.5 eV at 6 keV) over a 5 arcmin FoV.

The background for X-ray detectors accounts for several components: the diffuse X-ray photons, the soft protons ($<\sim$ 100 keV) funnelled by the mirrors, and the high energy particles ($>\sim$ 130 MeV) crossing the spacecraft and reaching the focal plane from every direction. An additional background component is due to the secondaries induced by these high energy particles along their path.

To estimate the impact of this latter component using a Monte Carlo simulation, three elements are required:

1. a representative mass model of the detector and its surroundings
2. a model of the environment expected in L2
3. a reliable set of physics models to describe the interaction of the environment with the mass model.

All these elements, in part also addressed inside the AREMBES project (ESA CTP), are part of the baseline X-IFU background evaluation activity. A highly detailed mass model of the X-IFU instrument and of its cryostat has been produced, a new model for the Galactic Cosmic Ray protons in L2 has been developed from satellite data, and a set of physics models tuned to ATHENA needs has been refined through extensive validations against experimental results. All these activities have allowed to reduce the uncertainty level associated with the simulations results.

In this paper we are going to report the latest results obtained after the update of all the elements of the Geant4 simulations and of the post processing software.

Further author information:
E-mail: simone.lotti@iaps.inaf.it, Telephone: +39 4993 4690

Space Telescopes and Instrumentation 2018: Ultraviolet to Gamma Ray, edited by Jan-Willem A. den Herder, Shouleh Nikzad, Kazuhiro Nakazawa, Proc. of SPIE Vol. 10699, 106991Q · © 2018 SPIE
CCC code: 0277-786X/18/$18 · doi: 10.1117/12.2313236

All the solutions adopted to reduce the background level (anticoincidence detector, passive shieldings) have been tested in the new configuration, with the aim to reach the scientific requirement of $5\times10^{-3}\ cts\ cm^{-2}s^{-1}keV^{-1}$. Furthermore, additional information regarding the angular distribution of background-inducing particles has been introduced and analyzed, together with energy of the primary particles generating unrejected background.

2. ENVIRONMENT MODEL

Our previous protons spectral model was the CREME96 maximum GCR spectrum,[1–3] representing the worst case, that was based on data measured in 1987. Starting from there a new study has been performed inside the ATHENA team to verify this assumption and derive a new reference model for the L2 environment.[4,5]

We performed an analysis of data from the Neutron Monitor stations to verify the assumption that 1987 was the worst case flux, and thanks to the wider temporal coverage of the data we found out that the highest flux ever measured since the sixties actually occurred in 2009 (with negative solar polarity), due to an exceptional minimum in the solar magnetic activity.

From here onward we decided to adopt the 2009 year as the worst case flux. This value, being the highest flux ever measured, represents the most conservative estimate for the flux that will be experienced by ATHENA during its mission lifetime. Further, the negative polarity is the one expected during the ATHENA lifetime.

A deep investigation of the data measured during 2009 has been performed. For this purpose, we have taken into account the data of Voyager2, PAMELA and SOHO, and compared them with the upper limit given by the CREME96 solar minimum.

The available data for 2009 cover the 0.3-1.6 GeV energy range, while we need the GCR spectrum from few MeV to several tens of GeV. To obtain the full spectrum we have referred to Usoskin work,[6,7] where the differential intensity J of cosmic ray nucleon at 1 AU in $p\ cm^{-2}s^{-1}sr^{-1}GeV^{-1}$ is given as:

$$J(T,\Phi) = J_{LIS}(T+\Phi)\frac{T(T+2T_r)}{(T+)(T++2T_r)} \tag{1}$$

where:

$$J_{LIS}(T) = \frac{1.9\times10^4(T(T+2T_r))^{-\frac{2.78}{2}}}{1+0.4866(T(T+2T_r))^{-\frac{2.51}{2}}} \tag{2}$$

is the Local Interstellar Spectrum (LIS) of cosmic ray nuclei and Φ is the modulation potential in GV, also known as the force field parameter and the modulation strength, and represents the mean energy loss of the GCR particle inside the heliosphere. T is the energy of the particle in GeV and $T_r = 0.938$ GeV is the proton rest mass.

Fitting together the datasets from SOHO, PAMELA and the one from Voyager2 rescaled at 1 AU with equation 1, we have obtained the best fit curve shown in Figure 1. The reduced χ^2 value obtained fitting this dataset is 1.84 with 94 degrees of freedom, while the value of Φ obtained is 379.3 MV (assuming $e^- = 1$). The best fit is strongly constrained by PAMELA data, given the lower errors and the wider energy coverage with respect to SOHO and Voyager2 ones.

The input spectrum for alpha particles has been evaluated from Kuznetsov empirical model[8] for quiet sun conditions, as:

$$F_{He} = 10^4E^{-2.72}\frac{E}{E+817}^{3.7} \tag{3}$$

where E is in MeV, and F_{He} in $p\ cm^{-2}s^{-1}sr^{-1}MeV^{-1}$.

Finally, the electrons spectrum was taken from Perinati[9] as:

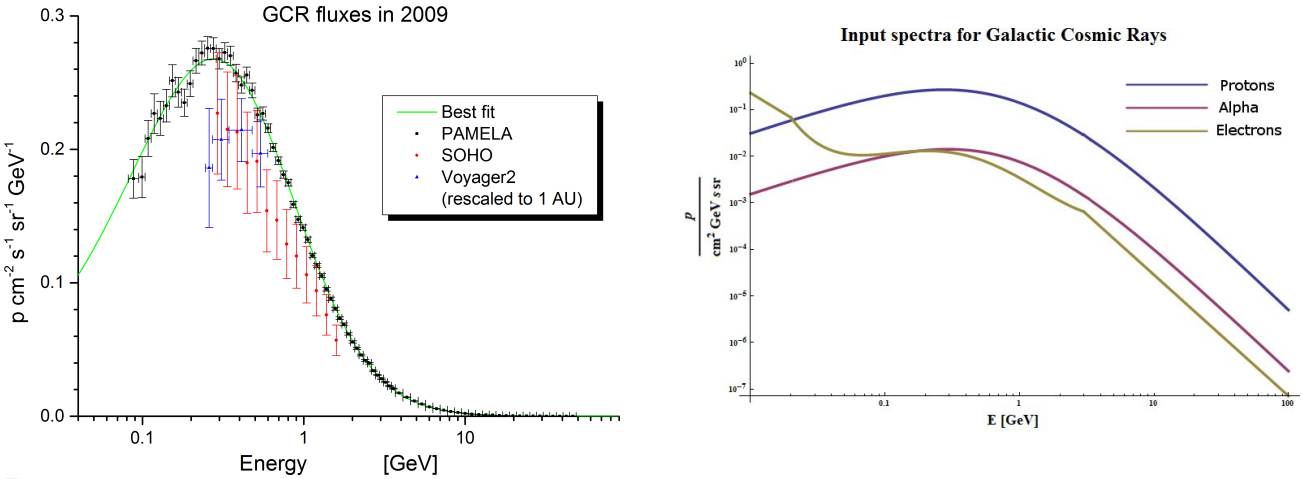

Figure 1: The best fit curve (in green) obtained by the datasets from PAMELA, SOHO and Voyager2 (Left). The input spectra for GCR protons, alpha particles and electrons used in the simulations (Right).

$$F_e = \begin{cases} \frac{0.000719}{10*E^{-1.75}}, & \text{if } E < 0.02 \text{ GeV} \\ 0.1\ exp[-3.37 - 1.6\ log(E) - 0.263\ log^2(e) + 0.238\ log^3(E) + 0.064\ log^4(E)], & \text{if } 0.02 < E < 3 \text{ GeV} \\ 0.0113E^{-2.6}, & \text{if } E > 3 \text{ GeV} \end{cases} \quad (4)$$

where E is in GeV, and F_{He} in $p\ cm^{-2}s^{-1}sr^{-1}GeV^{-1}$. All the spectra are shown in Figure 1 (Right).

3. MASS MODEL

With respect to the mass model described in our previous work,[10] we received an updated model of the cryostat from CNES on 9/5/2017 and an updated FPA model from SRON on 23/5/2017, from which we derived an updated version of the Geant4 mass model following the same procedure (see Figure 2).

With respect to the previous mass model, beside the revision of the structures surrounding the detector, we updated the TES absorbers thicknesses from 4 μm to 4.2 μm for Bismuth, and from 1 μm to 1.7 μm for Gold, inserted a more realistic model of the thermal filters, and the aperture cylinder sustaining them.

As for the previous version of the mass model, the different solids were assigned to different regions within Geant4, each with different settings of the cut for the generation of secondary particles:

- The detector, the supports, and the surfaces directly seen by the detector were assigned to the "inner region" with the lowest possible cut values (few tens of nm, high detail level)
- The remaining solids in the FPA were assigned to an "intermediate region" with higher cut values (few μm)
- The cryostat and the masses outside the FPA were assigned to the "external region" were the cut (few cm) allowed the creation only of high energy secondary particles

With this improved mass model as baseline we tested different FPA configurations to assess the expected background level: first of all, we tested the background level expected without any solution to reduce the background level. We then tested the effect of inserting the Cryogenic Anticoincidence (CryoAC) detector, and the passive Kapton shielding. Finally we test the effectiveness of two improved designs of the passive shield: one, already identified in previous work,[10] where the shield is a bilayer of 20 μm Bismuth and 250 μm Kapton, and the other where Bismuth is replaced with 10 μm of Gold, a material more suited to cryogenic applications.

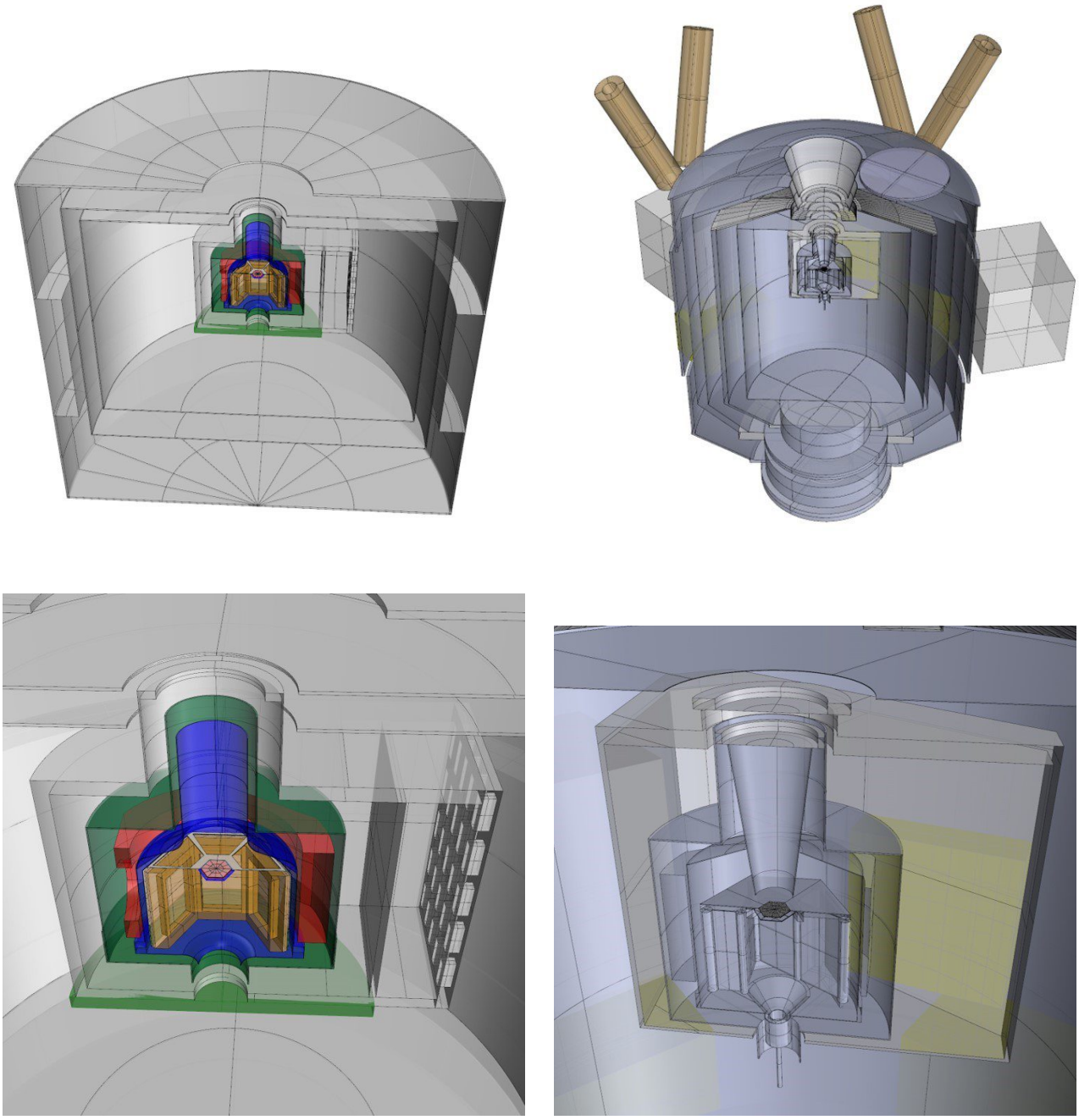

Figure 2: The old and new cryostat mass models (top left and right, respectively) and FPA (bottom left and right).

4. SIMULATIONS SETTINGS

Our team actively contributed to the definition of a new set of physics settings (Physics List) optimized for X-ray space applications and specifically tuned to ATHENA needs, the so called "Space Physics List" (SPL). The SPL was developed by the AREMBES collaboration with the aim to be included in the next Geant4 release, validating the physical processes relevant to the X-IFU and WFI instruments background against available experimental results, and has been officially endorsed by ESA, becoming the reference set of settings for the ATHENA Monte Carlo simulations. The Geant4 version used in the simulations with the SPL is 10.2.

5. NORMALIZATION PROCEDURE

If the Geant4 input source is a flux, the simulation normalization is intended as the process that leads from the number N of emitted particles to a particle or count rate in particles s^{-1} or counts s^{-1}, which requires the evaluation of the simulated equivalent exposure to the input flux.

The normalization procedure has recently been debated in the ATHENA collaboration, and finally the following procedure, firstly published in Fioretti (2012)[11] and reported in Fioretti (2018),[12] has been agreed upon by ESA and the ATHENA team.

If the particles are emitted from a spherical surface of radius r_{ext} enclosing the spacecraft following a cosine law angular distribution, then the simulated exposure time T (in seconds) to the isotropic flux depends on the number of simulated particles N as follows:

$$T = \frac{N}{\Phi \times 4\pi r_{ext}^2} \text{ seconds} \tag{5}$$

Where Φ is the input particles intensity in $p\ cm^{-2}s^{-1}sr^{-1}$. The instrumental detector count rate R is then obtained by dividing the number of detected counts C by the exposure time T, as $R = C/T\ cts\ s^{-1}$

The particle-induced background in the detector (e.g.,relative to the scientific signal) is the count rate per unit surface of the detector. In this case, the background is defined relative to the scientific signal and therefore, as only one side of the detector is usually exposed to the scientific signal,the surface S to be considered is the area of only one side of the detector. The background count rate per unit area, or background flux, of the detector B is therefore simply obtained as $B = R/S\ cts\ cm^{-2}s^{-1}$.

Conversely, in case the detector receives scientific signal from the whole detector surface exposed to the particle flux Σ, as would be the case of an anticoincidence shielding system surrounding the focal plane or a radiation monitor, the detected particle flux would be given by $F = R/\Sigma\ cts\ cm^{-2}s^{-1}$.

Finally, the energy averaged background flux (or particle flux) of the sensor in terms e.g., of $cts\ cm^{-2}s^{-1}keV^{-1}$. This can be obtained by dividing the background (or particle) flux by the operating energy range.

6. RESULTS

With the above premises, we proceeded to simulate the different configurations listed in Section 3, using GCR protons as input flux (since they constitute $\sim 90\%$ of the input particle flux). The resulting different background levels are reported in Figure 3 (left). We can see that without any solution to reduce it the X-IFU would experience a background level of 0.185 $cts\ cm^{-2}s^{-1}keV^{-1}$ in the 2-10 keV energy band, 37 times above the requirement of $5 \times 10^{-3}\ cts\ cm^{-2}s^{-1}keV^{-1}$.

The insertion of the CryoAC detector allows to reduce the background level down to $6\times10^{-3}\ cts\ cm^{-2}s^{-1}keV^{-1}$, 20% above the required level. This reduction is achieved effectively removing all the particles (primaries and secondaries) that are able to cross the main detector and reach the anticoincidence detector, such as MIPs, whose typical shape is no longer present in the spectrum.

The remaining unrejected background is induced mostly by secondary electrons created in the structures surrounding the detector, that either gets absorbed into the detector or bounces off its surface. To damp their contribution we shield the detector on its sides with a low secondary electrons yield material, such as Kapton, and this allows us to reduce the background level by 25%, reaching $4.5 \times 10^{-3}\ cts\ cm^{-2}s^{-1}keV^{-1}$. To further improve the shielding we decided to insert a 20 μm Bismuth layer before the Kapton, in order to shield the 16 keV fluorescence line emitted by the Niobium. This improvement also helped in further reducing the secondary electrons flux towards the detector, possibly due to the Niobium blocking a fraction of the activating flux towards the Kapton shield reaching a "optimal" background level of $3.7 \times 10^{-3}\ cts\ cm^{-2}s^{-1}keV^{-1}$. Backscattered electrons have repeatedly proven to be the main component of the residual background, since $\sim 85\%$ of the residual background is induced by secondary electrons, and $\sim 80\%$ of these electrons are backscattered, and therefore dedicated studies to this process have been performed.[13]

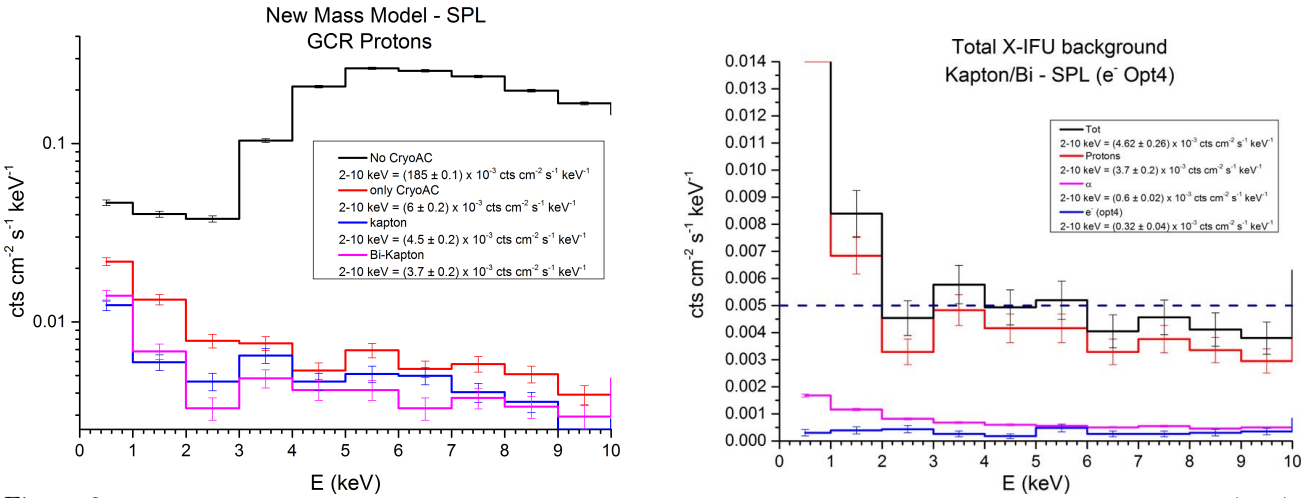

Figure 3: Unrejected X-IFU background levels in different configurations obtained with the Space Physics List (Left). The total unrejected background level (GCR Protons, alpha particles and e^-) in the Kapton/Bi configuration (Right).

Once this optimal configuration has been defined for protons, we moved on and simulated the remaining components of the L2 environment, obtaining the complete X-IFU background evaluation shown in Figure 3 (right). Even though alpha particles flux is $\sim 5\%$ of the protons one, their contribution to the background level amounts to $\sim 10\%$ with respect to the protons one. Similarly electrons flux is $\sim 3\%$ but their contribution is $\sim 8\%$.

We also improved the information output provided by the simulation, inserting additional information regarding the initial energy of the particles able to reach the detector, and the incident (and scattered) direction of the particle. Thanks to these information we were able to identify the energy ranges in which the different particle populations are contributing to the background (see Figure 4, left). We can see that heavier particles require higher energies to be able to reach the innermost part of the cryostat. Moreover, we were able to produce an angular distribution of the backscattered electrons. These particles impact on the detector surface and bounce back, releasing a small fraction of their energy (dependent on the impact angle). As it can be seen from Figure 4 (right), almost no electrons backscatter on the lower side of the detector, as the CryoAC efficiently blocks/vetoes those particles, while the major contribution comes from above, as expected. The distribution itself is quite flat, indicating no preferential direction from where these electrons come from, aside from a dip around the direction normal to the detector surface. An analysis of the FPA geometry reveals that this is roughly the FoV opening angle, the direction where there is almost no mass to produce the secondary electrons.

After having evaluated the total background level with the Kapton/Bi configuration, we tried to find an alternative solution to the use of Bismuth, since it is a particularly difficult to handle material. Together with SRON we decided to test the feasibility of Gold as a substitute material. As it was for the Bismuth, we calculated the thickness required to stop the 16 keV fluorescence from Niobium, and substituted the 20 μm Bismuth layer with 10 μm of Gold, and run a new simulation with GCR protons. The results are shown in Figure 5. As it can be seen, the resulting integrated background level is compatible with the one obtained with Bismuth, but the gold fluorescence line at 9.8 keV emerged in the background. This does not pose sensible issues, since the Gold line is already expected from a few structures that is not possible to recreate in the simulation, and moreover it is placed at the very edge of the instrument sensitivity band. We therefore remark the Kapton/Au configuration as feasible for the implementation.

7. CONCLUSIONS

Thanks to the adoption of active and passive solutions to reduce the particle background, we estimated the X-IFU background level in the "optimal" configuration to be $\sim 4.6 \times 10^{-3}$ $cts\ cm^{-2}s^{-1}keV^{-1}$ (GCR protons, alpha particles and electrons included), slightly below the scientific requirement of 5×10^{-3} $cts\ cm^{-2}s^{-1}keV^{-1}$.

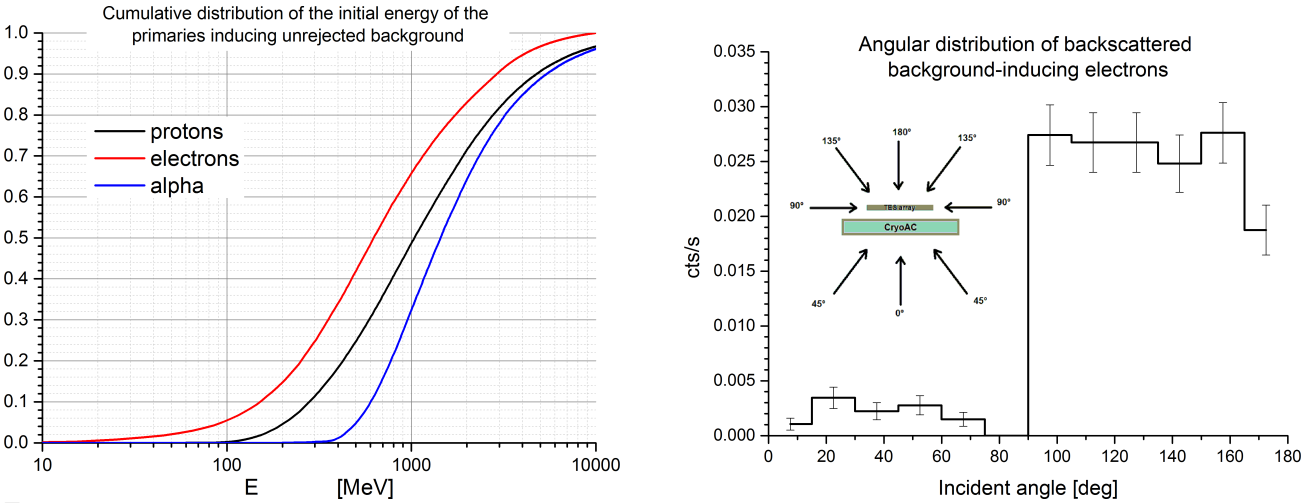

Figure 4: Cumulative distribution of the initial energies of the particles able to reach the detector and induce unrejected background (Left). Angular distribution of the secondary electrons backscattering on the detector surface and inducing background in the 2-10 keV energy band (Right).

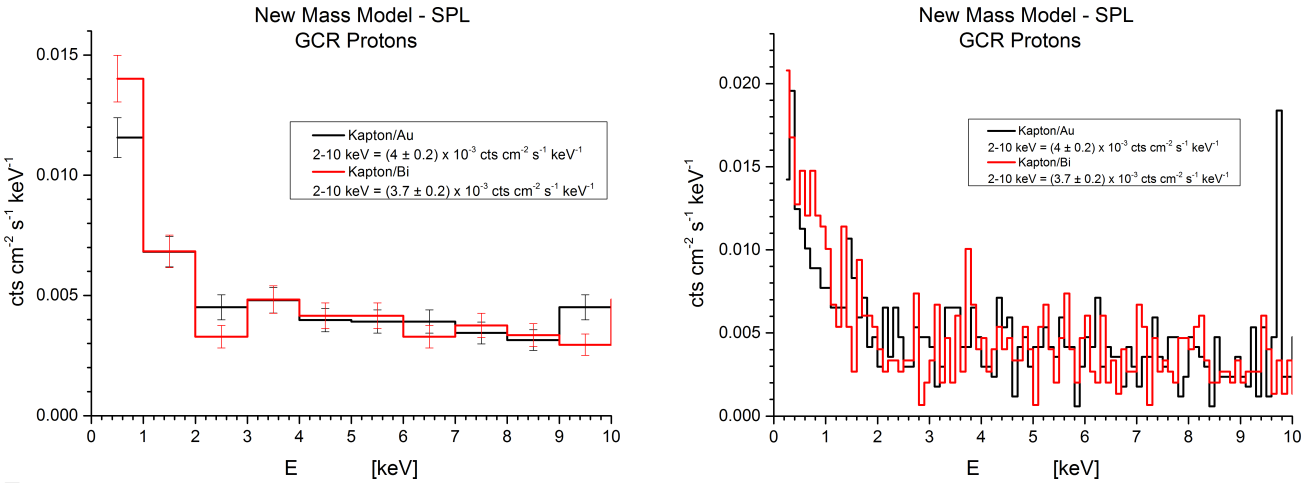

Figure 5: The unrejected background spectra obtained with the Kapton/Bi and Kapton/Au configurations. 1 keV energy bins (Left, to highlight the continuum), and 100 eV bins (Right, to highlight fluorescences).

This result was obtained with the most up-to-date mass model, under the conservative assumption of assuming the worst particle environment conditions (see Section 2).

Backscattered electrons have repeatedly proven to be the major component of the unrejected background for X-IFU ($\sim 70\%$), as soon as the high energy component of the background is removed by the CryoAC. The angular distribution of these particles has been investigated, and proven to be flat for directions outside the instrument FoV.

The energy range in which the different particle species contribute to the background has been identified. This information allows us to understand particles which energy range we have to monitor outside of the satellite, since spectral changes outside the energy range identified will not affect the background level. This can be used to derive the requirements for a dedicated particle monitor that will measure the external fluxes experienced by the mission.

Finally we identified an alternative solution with respect to the "optimal" configuration, that allows to obtain compatible background levels, but using Gold instead of Bismuth, the former being a much easier to handle material.

ACKNOWLEDGMENTS

The research leading to these results has received funding from the European Unions Horizon 2020 Programme under the AHEAD project (grant agreement n. 654215). The ESA Contract No. 4000116655/16/NL/BW (AREMBES project) and ASI contract no. 2015-046-R.0 are acknowledged. The authors wish to thank the Centre National d'Etudes Spatiales for providing the computing power required to perform part of the Monte Carlo simulations presented in this study.

REFERENCES

[1] Tylka, A. J., Adams, J. H., Boberg, P. R., Brownstein, B., Dietrich, W. F., Flueckiger, E. O., Petersen, E. L., Shea, M. A., Smart, D. F., and Smith, E. C., "Creme96: A revision of the cosmic ray effects on micro-electronics code," *IEEE Trans. Nucl. Sci.* **44**, 2150–2160 (1997).

[2] Weller, R. A., Mendenhall, M. H., Reed, R. A., Schrimpf, R. D., Warren, K. M., Sierawski, B. D., and Massengill, L. W., "Monte carlo simulation of single event effects," *IEEE Trans. Nucl. Sci.* **57**, 1726–1746 (2010).

[3] Mendenhall, M. H. and Weller, R. A., "A probability-conserving cross-section biasing mechanism for variance reduction in monte carlo particle transport calculations," *Nucl. Inst. & Meth. A* **667**, 38–43 (2012).

[4] Minervini, G. and Lotti, S., "Consolidation of the absolute level of the Galactic Cosmic Ray (GCR) protons spectrum and its uncertainty at L2 during the ATHENA mission lifetime (2028-2033)," *Technical Note* (2018).

[5] Minervini, G., Lotti, S., Macculi, C., Piro, L., Laurenza, M., Molendi, S., D'Andrea, M., and Argan, A., "Proton Cosmic Ray foreseen in L2 orbit duting the ATHENA lifetime," *In preparation* (2018).

[6] Usoskin, I. G., Huotari, K. A., Kovaltsov, G. A., and Mursula, K., "Heliospheric modulation of cosmic rays: Monthly reconstruction for 19512004," *Journal of Geophysical Research* **110** (2005).

[7] Usoskin, I. G., Bazilevskaya, G. A., and Kovaltsov, G. A., "Solar modulation parameter for cosmic rays since 1936 reconstructed from ground-based neutron monitors and ionization chambers," *Journal of Geophysical Research* (2011).

[8] Kuznetsov, N. V., Popova, H., and Panasyuk, M. I., "Empirical model of longtime variations of galactic cosmic ray particle fluxes," *Journal of Geophysical Research: Space Physics* **122** (2017).

[9] Perinati, E., Tenzer, C., Santangelo, A., Dennerl, K., Freyberg, M., and Predehl, P., "The radiation environment in l-2 orbit: implications on the non-x-ray background of the erosita pn-ccd cameras," *Experimental Astronomy* **33** (2012).

[10] Lotti, S., Mineo, T., Jacquey, C., Molendi, S., DAndrea, M., and C. Macculi, L. P., "The particle background of the x-ifu instrument," *Experimental Astronomy* **44** (2017).

[11] Fioretti, V. et al., "The low earth orbit radiation environment and its impact on the prompt background of hard x-ray focusing telescopes," *Proc. of SPIE* **8453**, 845331 (2012).

[12] Fioretti, V., Lotti, S., and Santin, G., "AREMBES WP 7: Normalization of an isotropic flux in space in Geant4 simulations," *ESA AREMBES TN* (2018).
[13] Dondero, P., Mantero, A., Ivanchencko, V., Lotti, S., Mineo, T., and Fioretti, V., "Electron backscattering simulation in geant4," *Nucl.Instrum.Meth. B* **425** (2018).